Hot Giant Fullerenes Eject and Capture C2 Molecules: QM/MD Simulations with Constant Density

3 AUTHORS:

Biswajit Saha
36 PUBLICATIONS   494 CITATIONS

SEE PROFILE

Stephan Irle
Nagoya University
203 PUBLICATIONS   3,264 CITATIONS

SEE PROFILE

Keiji Morokuma
Fukui Institute for Fundamental Chemistry
442 PUBLICATIONS   13,770 CITATIONS

SEE PROFILE

Hot Giant Fullerenes Eject *and* Capture C₂ Molecules: QM/MD Simulations with Constant Density

Biswajit Saha,[†,§] Stephan Irle,[*,‡] and Keiji Morokuma[*,†,§]

[†]Fukui Institute for Fundamental Chemistry, Kyoto University, Kyoto 6068103, Japan

[‡]Institute for Advanced Research and Department of Chemistry, Nagoya University, Nagoya 464-8602, Japan

[§]Cherry L. Emerson Center for Scientific Computation and Department of Chemistry, Emory University, Atlanta, Georgia 30322, United States

S *Supporting Information*

ABSTRACT: Quantum chemical molecular dynamics (QM/MD) simulations using periodic boundary conditions show that hot giant fullerene (GF) cages can both eject and capture C_2 molecules dependent on the concentration of noncage carbons in the simulated system, and that the cage size can therefore both increase and decrease under high temperature conditions.

The reaction mechanisms for C_2 elimination and incorporation involve sp^3 carbon defects and polygonal rings larger than hexagons, and are thus closely related to previously described mechanisms (Murry, R. L.; Strout, D. L.; Odom, G. K.; Scuseria, G. E. *Nature* **1993**, *366*, 665). The atoms constituting the cage are gradually replaced by the two processes, suggesting that a fullerene cage during high-temperature synthesis is a dissipative structure in the sense of Ilya Prigogine's theory of self-organization in nonequilibrium systems. Explicit inclusion of Lennard-Jones-type helium or argon noble gas atoms is found to increase the GF shrinking rate. Large GFs shrink at a greater rate than small GFs. The simulations suggest that in an idealized, *closed* system the fullerene cage size may grow to a dynamic equilibrium value that depends on initial cage size, temperature, pressure, and overall carbon concentration, whereas in an *open* system cage shrinking prevails when noncage carbon density decreases as a function of time.
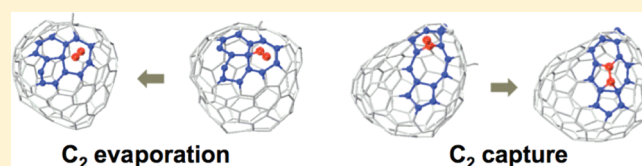
1. INTRODUCTION

Research to understand the fullerene formation and growth mechanism and the high yield of buckminsterfullerene (BF) C_{60} continues to this date, more than 25 years after the prediction of the famous truncated icosahedron structure by Smalley, Kroto, Curl, and co-workers.[1] Current spectroscopic techniques do not allow the identification of intermediate structures along the path from hot chaotic carbon vapor or hydrocarbon combustion flame species to the highly symmetric, spherical BF cage. At the same time, no real-time atomistic theoretical simulation has been able to reproduce the experimentally observed abundance pattern of fullerene cage size isomers as shown for instance in ref 2. On the basis of fragmentary experimental findings, several hypothetical fullerene formation mechanisms have been formulated in the past,[3−8] most prominent among them the "party line" mechanism,[3] the "pentagon road",[7] and the "ring fusion spiral zipper" mechanism.[8] None of these hypothetical mechanisms has been strictly confirmed, and none considered explicitly the effect of rapid cooling and gas expansion, driving the reaction systems far away from thermodynamic equilibrium to a nonequilibrium domain where highly ordered, dissipative structures can self-organize in an otherwise chaotic environment.[9−12] A recent study by Curl et al.[13] assumed to the contrary that the carbon clusters are in thermal equilibrium with each other.

To directly simulate the fullerene formation process, we had performed earlier a series of density-functional tight-binding (DFTB)[14,15]-based quantum chemical molecular dynamics

(QM/MD) simulations.[16−22] These extensive nonequilibrium MD studies led to the formulation of the "shrinking hot giant" (SHG) road of fullerene formation,[20,21,23] according to which at first giant fullerenes (GFs) C_n with $n > 80$ self-assemble through irreversible interactions and autocatalytic reactions of polyyne chains or macrocycles ("size up"), which then shrink in size down to smaller, kinetically more stable fullerenes such as C_{70} and C_{60}, initially by polyyne "antenna" "falloff" and later by continued and irreversible C_2 evaporation ("size down").[19,23] The latter cage shrinking process resembles Smalley's "shrink-wrap" mechanism of laser-induced C_2 elimination from C_{60},[7,24] and occurs under the effect of thermal excitation in the case of defect-bearing fullerene cages, even though the shrinking process itself is endothermic.

The dynamic self-assembly mechanism of GFs,[25,26] and the importance of the GF shrinking process for the high abundance of BF in theoretical studies[27−30] has recently been confirmed by other groups. For instance, an innovative pulsed microplasma cluster source (PMCS) experiment showed that if no external heat for annealing was provided, monotonically *increasing* fullerene abundance with cluster size results. In the mass spectra of this PMCS experiment, C_{60} and C_{70} exhibit no special abundance,[25] and the resulting monotonically increasing abundance

pattern appears to be in agreement with thermodynamic considerations.[31,32] On the other hand, as shown by Smalley, Kroto, Curl et al., higher buffer gas pressure and especially prolonged heating changes the abundance pattern and leads to the high abundance of C_{60} and C_{70}.[1] Thus, it is not surprising that carrier gas-carbon cluster and cluster—cluster collisions occurring at optimal pressure play a key role in the GF shrinking process.[33] All these observations are in line with a high-temperature annealing process that changes the initial abundance spectrum of fullerene isomers. And indeed, the shrinking of a GF molecule containing 1300 carbon atoms over the course of 800 s down to C_{60} and eventual cage destruction has been observed experimentally in an HRTEM movie,[34] lending support for the thermal C_2 evaporation process as part of the SHG road of fullerene formation.

Although thermal shrinking has been established as a widely accepted mechanism, recent HRTEM observations of direct fullerene formation from a graphene flake[35] and of catalyst-free fullerene growth inside nanotubes,[36] as well as the symmetric smooth size distributions of fullerene laser coalescence products around main BF dimer (C_{118}), trimer (C_{178}), etc. peaks[37] are seemingly at odds with the SHG road. We note, however, that in the cage growth[36] and coalescence[37] experiments a *tightly sealed environment* is required, and that C_2 can presumably not escape in such an experimental setup. It therefore appears that in addition to C_2 evaporation, the reverse process, namely C_2 capture, should occur as well, consistent with the principle of microscopic reversibility. Curl and co-workers based their "spreading the distribution" mechanism on C_2 exchange between fullerene cages to explain the experimentally observed abundance patterns.[13] Such line of thinking follows an earlier theoretical work by Yi et al. who reported a possible $C_{58} + C_{62} \rightarrow 2C_{60}$ comproportionation mechanism.[38] Their kinetic modeling predicted fullerene abundance spectra that bear similarity to those from experiment.[13] However, caution should be used when interpreting experimentally obtained fullerene abundance distributions: the abundance envelope of fullerene cages in time-of-flight (TOF) mass spectrometry study based on laser desorption (LD) is sensitive to chemical reactions induced by the *desorption* laser, such as shrinking and oligomerization processes.[39,40]

We now turn our attention to possible C_2 insertion mechanisms. In 1992, Endo and Kroto[41] simply proposed a reversal of a C_2 elimination mechanism that had been introduced by O'Brien et al. in the context of their laser-induced fullerene shrink-wrap experiments.[7,24,42] The structural motif accepting the C_2 unit to produce a fused pentagon pair was named "Endo—Kroto patch", and is shown in Scheme 1 a. Saito et al.[43] and Yoshida and Osawa[44] postulated an asymmetric pathway as depicted in Scheme 1 b, producing an intermediate heptagon, which can potentially heal the energetically unfavorable abutting pentagon pair of the Endo—Kroto patch. Although it was immediately realized that the Endo—Kroto insertion mechanism (Scheme 1 a) is Woodward—Hoffmann forbidden,[41] that the production of the abutting pentagon pair is energetically highly unfavorable,[45] and that the absence of a stabilization in the transition state geometry should lead to the immediate loss of the attaching C_2 unit,[44] the Endo—Kroto insertion patch was rather popular and is still cited and/or used in the context of catalyst-free nanocarbon structure growth.[46−48] This is so despite the fact that quantum chemical investigations of the Endo—Kroto-type transition state structures by Budyka et al.[49,50] confirmed that the C_2 unit would immediately be expelled again

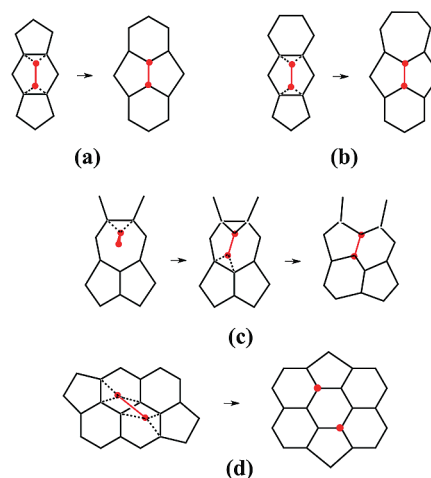Scheme 1. Mechanism of C_2 Insertion into Fullerene (a) According to Reference 41 and (b) According to Reference 44

(a)   (b)

(c)

(d)

Table 1. Lennard-Jones Potential Used for Diatomic Interactions with Ng Participation in the Present Simulations

atom pair	ε_{ij} (kJ/mol)	σ_{ij} (Å)
C—He	0.013 5072[a]	2.740[a]
He—He	0.083 6820[b]	2.556[b]
C—Ar	0.480 4704[c]	3.380[c]
Ar—Ar	0.996 6384[c]	3.400[c]

[a] Reference 57. [b] Reference 58. [c] Reference 59.

due to the excess energy provided by the addition energy. Apparently, as Yi et al. found earlier in Car—Parrinello molecular dynamics simulations,[38] the initial orientation of the attacking C_2 unit seems important: only if both ends simultaneously attach to the cage, the danger of losing the newly added fragment, highlighted in ref 50, might be overcome. Such a conformation of attack has a low probability, and indeed an LDTOF-MS study, also reported in the same reference, confirmed that primary adducts with formal C_{62} composition are unstable and decompose back to C_{60} by C_2-fragment emission. We note that in this LDTOF-MS experiment the environment was not sealed and C_2 could have escaped the reaction environment.

As an energetically more favorable alternative to Endo—Kroto-type reactions, Scuseria and co-workers suggested in 1993 stepwise insertion pathways that involved sp^3-carbon defects as well as heptagons and larger polygons,[51−53] a prototypical one being depicted in Scheme 1 c. However, this particular stepwise C_2 addition to a heptagon fused to two abutting pentagons was criticized as too unlikely to occur, since a 7/5/5 defect with abutting pentagon pair would have to be created first.[44] As another alternative to the Endo—Kroto patch insertion, Saito et al. had proposed a dissociative addition pathway, where the incoming C_2 unit immediately suffers cleavage of the C—C bond. Their proposed pathway is shown in Scheme 1 d, but this reaction pathway was also dismissed as "chemically unacceptable".[49,54]

In the present study we therefore revisit the size-down shrinking process of hot GFs as well as the growth mechanism by maintaining constant carbon density in a QM/MD simulation with periodic boundary conditions, to simulate the effect of an environment where C_2 cannot escape. In contrast, our previous

QM/MD simulations of cage shrinking were performed in vacuum, where the carbon density was allowed to decrease over time.[19,23] Additionally, here we explicitly include noble gas (Ng) atoms in the model system to increase the pressure. Interactions with Ng atoms were included using nonbonded molecular mechanics Lennard-Jones potentials, resulting in the use of a mixed QM/MM potential. We describe details of isokinetic, high-temperature QM/MD trajectories for C_2 ejection and capture processes of GFs that were self-assembled in previous simulations,[22,55] and focus on the structure and energetics of "antenna fall-off", "C_2 pop out", and "C_2 incorporation" events under the constant density conditions. Our study is qualitative and not aimed at quantitatively evaluating shrinking and growth rates and their dependence on fullerene cage isomer, carbon density, buffer gas pressure, and temperature, as such a study would exceed present computational capabilities, using the MD approach.

2. COMPUTATIONAL METHODOLOGY

2.A. DFTB QM and QM/MM Potentials. Molecular dynamics (MD) simulations were performed using the density-functional tight-binding (DFTB) method as implemented in the program package developed by Frauenheim, Seifert, Elstner, and co-workers.[14,15,56] DFTB is an approximate density functional theory method based on the tight binding approach and uses an optimized minimal linear combination of atomic orbitals (LCAO) Slater-type valence-only basis set in combination with a two-center approximation for the Hamiltonian matrix elements. The non-charge-consistent (NCC) approximation of DFTB was adopted to obtain energies and nuclear gradients of all carbon structures. The Γ-point approximation was employed in the periodic boundary calculations. C−Ng and Ng−Ng interactions were evaluated using Lennard-Jones (LJ) pair potentials. The C−He, He−He, C−Ar, and Ar−Ar LJ parameters were taken from references 57−59 and are given in Table 1.

2.B. Molecular Dynamics Simulations. Direct QM/MD trajectories were generated by calculating analytical DFTB energy gradients on the fly using a Verlet integrator, applying a time integration interval Δt of 0.48 fs. We performed two sets of simulations: one in the microcanonical (NVE) ensemble where we include explicit buffer gas atoms to increase the atom density (pressure) and act as a heat bath, the other by applying a velocity scaling thermostat (NVT) and no buffer gas atoms. The Cartesian coordinates and atomic velocities for GFs (GF_n, where n = 1, 10) obtained in our previous simulations were taken as starting points (reset t = 0.00 ps) for these trajectories[22,55] of benzene combustion. Specifically, GF_n (n = 1−5, 9, 10) correspond to cages obtained from trajectories B3000 kg1_1, B3000 kg1_2, B3000 kg1_3, B3000 kg2_7 and B3000 kg3_7, B3000 kg3_13, B3000 kg4_6, respectively, as reported in ref 22. The remaining GF_n (n = 6−8) correspond to fullerenes obtained from trajectories P3000K_7, P3000K_9, P3000K_10, respectively, as reported in ref 55. Noble gas atoms (500 He or 500 Ar atoms) were added in random initial positions in NVE simulations surrounding the GF in a cubic periodic boundary condition (PBC) box with a side length of 70 Å, keeping minimum atom−atom distance of 3.5 Å. Here, initial velocities equivalent to 3000 K were supplied to the buffer gas atoms according to the Maxwell−Boltzmann velocity distribution. We label the trajectories GF_n_x, where n = 1, 2,..., 10 denotes the trajectory number and x specifies either He or Ar. In the case of isokinetic NVT

Table 2. Number of Carbon Atoms on the Cluster (#$C_{cluster}$), on the Cage (#C_{cage}), and on the Antenna (#$C_{antenna}$), and the Root-Mean-Square Cage Curvature at 0 and 1210 ps

trajectory name	#$C_{cluster}$ 0 ps	#$C_{cluster}$ 1210 ps	#C_{cage} 0 ps	#C_{cage} 1210 ps	#$C_{antenna}$ 0 ps	#$C_{antenna}$ 1210 ps	rms curvature (1/Å) 0 ps	rms curvature (1/Å) 1210 ps
GF_1_VS	146	127	120	125	26	2	0.212	0.227
GF_1_He	146	128	120	128	26	0	0.212	0.246
GF_1_Ar	146	124	120	124	26	0	0.212	0.246
GF_2_VS	152	148	149	148	3	0	0.241	0.226
GF_2_He	152	148	149	148	3	0	0.241	0.243
GF_2_Ar	152	148	149	148	3	0	0.241	0.234
GF_3_VS	156	146	135	140	21	6	0.222	0.223
GF_3_He	156	132	135	132	21	0	0.222	0.236
GF_3_Ar	156	132	135	132	21	0	0.222	0.235
GF_4_VS	184	162	160	162	24	0	0.219	0.236
GF_4_He	184	158	160	156	24	0	0.219	0.243
GF_4_Ar	184	162	160	162	24	2	0.219	0.233
GF_5_VS	89	80	76	75	13	5	0.238	0.257
GF_5_He	89	79	76	77	13	2	0.238	0.273
GF_5_Ar	89	77	76	77	13	3	0.238	0.276
GF_6_VS	135	131	131	130	4	1	0.237	0.225
GF_6_He	135	123	131	122	4	1	0.237	0.241
GF_6_Ar	135	125	131	125	4	3	0.237	0.243
GF_7_VS	132	132	130	130	2	0	0.244	0.237
GF_7_He	132	118	130	118	2	4	0.244	0.238
GF_7_Ar	132	122	130	122	2	0	0.244	0.239
GF_8_VS	144	125	102	124	42	3	0.210	0.226
GF_8_He	144	118	102	118	42	0	0.210	0.250
GF_8_Ar	144	126	102	124	42	2	0.210	0.237
GF_9_VS	167	140	80	125	87	15	0.195	0.238
GF_9_He	167	123	80	119	87	4	0.195	0.225
GF_9_Ar	167	132	80	128	87	4	0.195	0.241
GF_10_VS	119	92	88	90	31	3	0.235	0.260
GF_10_He	119	88	88	88	31	0	0.235	0.267
GF_10_Ar	119	98	88	98	31	0	0.235	0.262

conditions, a target temperature of 3000 K was maintained by using a velocity scaling thermostat without buffer gas atoms. An overall scaling probability of 20% was employed. These trajectories are labeled with x = VS (velocity scaling thermostat). A total of 30 trajectories (10 NVE including He, 10 NVE including Ar, and 10 NVT simulations) were performed for up to 1210 ps.

3. RESULTS AND DISCUSSION

3.A. Phenomenological Description of the Trajectories. In the next sections we will use the following convention: The term "antenna" identifies initially existing polyyne chains attached to the fullerene cages as a result of the dynamic self-assembly process via ring condensation growth (for a detailed discussion see refs 19, 20, 22, 23). "Cluster" stands for an isolated carbon structure, usually a fullerene with "antenna". "Cage" denotes only the part of the cluster consisting of sp^2 carbon cage without "antenna". Initially, the sum of antenna and cage carbon atoms determines the cluster size, which is the total number of carbon

Table 3. Numbers of 5-, 6-, 7-, and 8-Membered Rings (#ring) in the Cage at 0 and 1210 ps, the Change in Ring Numbers Δ#ring = #ring (1210 ps) − #ring (0 ps), and Ratio of 6-Membered Rings (#6) to the Sum of Non-6-Membered Rings (#5 + #7 + #8) at 0 and 1210 ps

	#ring (5 | 6 | 7 | 8)			#6/(#5 + #7 + #8)	
trajectory name	0 ps	1210 ps	Δ#ring (5 | 6 | 7 | 8)	0 ps	1210 ps
GF_1_VS	15 | 35 | 10 | 1	18 | 39 | 6 | 1	+3 | +4 | −4 | +0	1.35	1.56
GF_1_He	15 | 35 | 10 | 1	13 | 52 | 1 | 0	−2 | +17 | −9 | −1	1.35	3.71
GF_1_Ar	15 | 35 | 10 | 1	14 | 48 | 2 | 0	−1 | +13 | −8 | −1	1.35	3.00
GF_2_VS	22 | 43 | 10 | 1	23 | 42 | 11 | 0	+1 | −1 | +1 | −1	1.30	1.24
GF_2_He	22 | 43 | 10 | 1	22 | 42 | 10 | 0	+0 | −1 | +0 | −1	1.30	1.31
GF_2_Ar	22 | 43 | 10 | 1	22 | 44 | 10 | 0	+0 | +1 | +0 | −1	1.30	1.38
GF_3_VS	25 | 30 | 8 | 3	22 | 37 | 10 | 2	−3 | +7 | +2 | −1	0.83	1.09
GF_3_He	25 | 30 | 8 | 3	20 | 40 | 8 | 0	−5 | +10 | +0 | −3	0.83	1.43
GF_3_Ar	25 | 30 | 8 | 3	23 | 35 | 9 | 1	−2 | +5 | +1 | −2	0.83	1.06
GF_4_VS	25 | 31 | 17 | 6	25 | 45 | 13 | 0	+0 | +14 | −4 | −6	0.65	1.18
GF_4_He	25 | 31 | 17 | 6	21 | 48 | 10 | 0	−4 | +17 | −7 | −6	0.65	1.55
GF_4_Ar	25 | 31 | 17 | 6	19 | 57 | 7 | 0	−6 | +26 | −10 | −6	0.65	2.19
GF_5_VS	11 | 19 | 7 | 5	13 | 22 | 1 | 2	+2 | +3 | −6 | −3	0.83	1.38
GF_5_He	11 | 19 | 7 | 5	14 | 22 | 4 | 0	+3 | +3 | −3 | −5	0.83	1.22
GF_5_Ar	11 | 19 | 7 | 5	16 | 19 | 4 | 1	+5 | +0 | −3 | −4	0.83	0.90
GF_6_VS	26 | 26 | 14 | 1	26 | 28 | 11 | 1	+0 | +2 | −3 | +0	0.63	0.74
GF_6_He	26 | 26 | 14 | 1	23 | 29 | 9 | 2	−3 | +3 | −5 | +1	0.63	0.85
GF_6_Ar	26 | 26 | 14 | 1	20 | 35 | 8 | 1	−6 | +9 | −6 | +0	0.63	1.21
GF_7_VS	23 | 27 | 11 | 4	23 | 32 | 9 | 3	+0 | +5 | −2 | −1	0.71	0.91
GF_7_He	23 | 27 | 11 | 4	14 | 38 | 6 | 0	−9 | +11 | −5 | −4	0.71	1.90
GF_7_Ar	23 | 27 | 11 | 4	18 | 32 | 9 | 1	−5 | +5 | −2 | −3	0.71	1.14
GF_8_VS	17 | 28 | 5 | 2	19 | 36 | 9 | 1	+2 | +8 | +4 | −1	1.17	1.24
GF_8_He	17 | 28 | 5 | 2	18 | 34 | 8 | 0	+1 | +6 | +3 | −2	1.17	1.31
GF_8_Ar	17 | 28 | 5 | 2	16 | 40 | 8 | 0	−1 | +12 | +3 | −2	1.17	1.67
GF_9_VS	16 | 16 | 4 | 5	15 | 44 | 5 | 1	−1 | +28 | +1 | −4	0.64	2.10
GF_9_He	16 | 16 | 4 | 5	14 | 35 | 7 | 0	−2 | +19 | +3 | −5	0.64	1.67
GF_9_Ar	16 | 16 | 4 | 5	18 | 39 |5 | 0	+2 | +23 | +1 | −5	0.64	1.70
GF_10_VS	11 | 25 | 5 | 1	16 | 27 | 4 | 0	+5 | +2 | −1 | −1	1.47	1.35
GF_10_He	11 | 25 | 5 | 1	17 | 24 | 5 | 0	+6 | −1 | +0 | −1	1.47	1.09
GF_10_Ar	11 | 25 | 5 | 1	13 | 34 | 2 | 0	+2 | +9 | −3 | −1	1.47	2.27

atoms present in the simulations. We note that each trajectory has therefore a different carbon density since the PBC box size is the same. Table 2 lists for carbon clusters present at beginning and end points of all 30 trajectories the cluster size ($\#C_{cluster}$), the number of cage carbon atoms ($\#C_{cage}$), the number of antenna carbon atoms ($\#C_{antenna}$), and the root-mean-square (rms) curvature of the fullerene cage. The structures and corresponding Cartesian coordinates of the carbon clusters at $t = 0$ ps and $t = 1210$ ps are also given in the Supporting Information. The rms curvature is defined as the average of inverse radii of spheres best fitted to an sp^2-carbon atom plus its three bonded neighbors, and the cage curvature is estimated only on the basis of the local curvature of the sp^2 cage carbon atoms.

All GFs possess initially antennas with $\#C_{antenna}$ ranging from 2 to 87. These GFs also possess other structural defects such as an odd number of cage atoms, fused pentagons, more than 12 pentagons, many heptagons, and some octagons (see Table 3). In all cases, $\#C_{cluster}$ (not necessarily $\#C_{cage}$) decreased as a result of antenna "falloff" and C_2 "pop-out" during high-temperature simulations. The dissociated carbon chains and C_2 units remained in the PBC box and provided the source for carbon

fragment capture, resulting in antenna reattachment. Such events could obviously not be seen in our previous simulations that were carried out in a vacuum.[19,23] We found that a GF cage may indeed grow by ingestion of carbon fragments that initially attach as "re-grown antennas" depending on a variety of factors. The cage size increases in all trajectories of model systems GF_1 ($\#C_{antenna} = 26$), GF_8 ($\#C_{antenna} = 42$), and GF_9 ($\#C_{antenna} = 87$), and decreases in all trajectories of model system GF_2 ($\#C_{antenna} = 3$). Other cases present mixed results under different NVT or NVE and pressure conditions, but we note that, in GF_3 ($\#C_{antenna} = 21$), GF_6 ($\#C_{antenna} = 4$), and GF_7 ($\#C_{antenna} = 2$), the NVE simulations with higher pressure lead to cage shrinking, while NVT simulations in the absence of Ng pressure exhibit no change or growth. The evolution of $\#C_{cluster}$ and $\#C_{cage}$ during the simulations are shown in Figure 1a,b for GF_1_x and GF_8_x, respectively, where cage size growth is prominent. Figure 1c,d shows the same cluster size evolution for trajectories GF_6_x and GF_7_x, where shrinking is seen in the presence of buffer gas. Equivalent figures for remaining trajectories are shown in the Supporting Information (Figures S1−S6). Each of these figures consists of three panels, the upper corresponds to the low
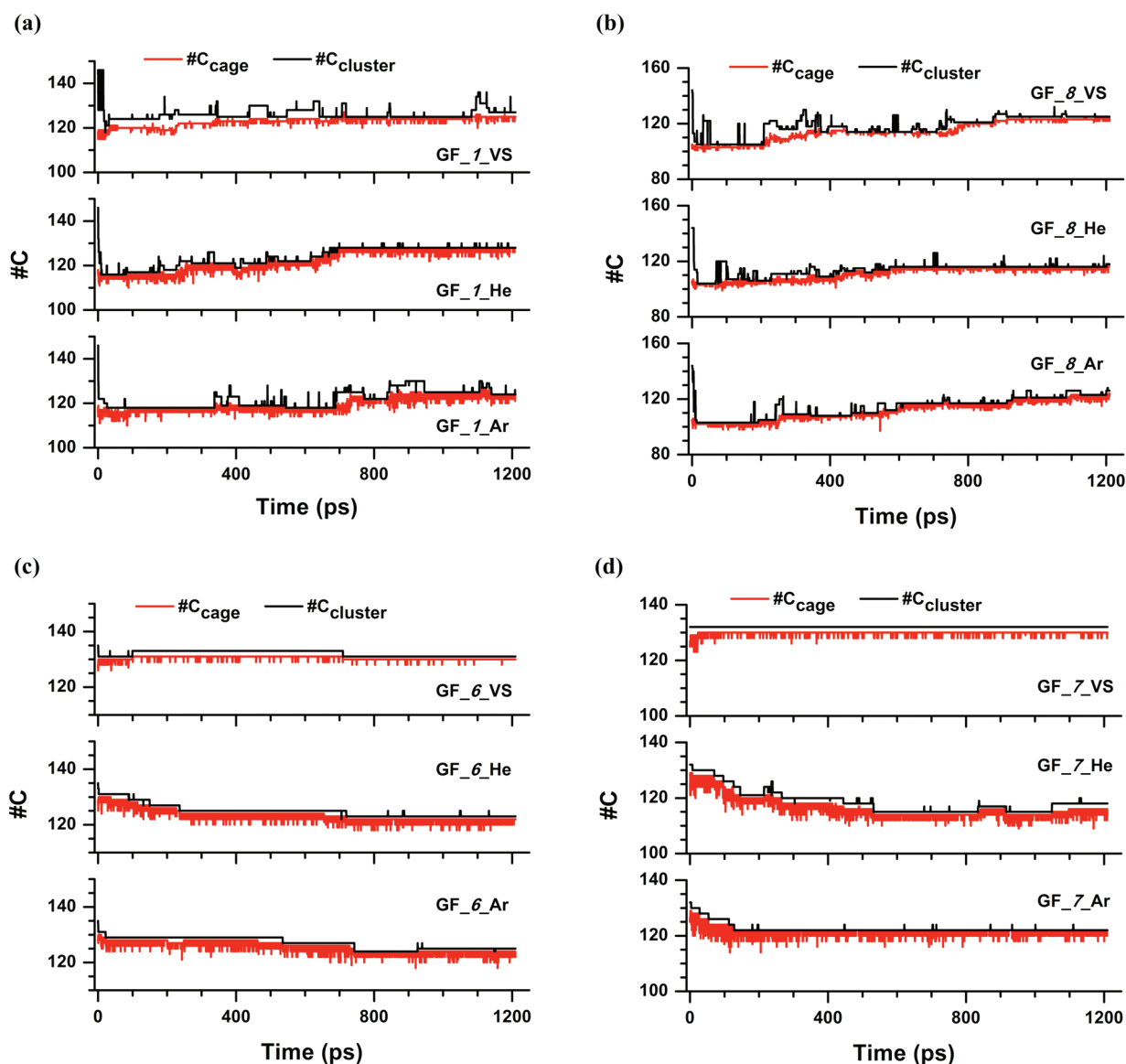
22710

dx.doi.org/10.1021/jp203614e |*J. Phys. Chem. C* 2011, 115, 22707–22716

Figure 1. Cluster and cage size evolution with different simulation conditions. Parts a and b represent cases where overall growth is observed. Overall shrinking is observed in parts c and d for NVE simulations with Ng pressure.

pressure NVT simulations denoted GF_n_VS, the middle to He pressure NVE simulations denoted GF_n_He, and the lower to Ar pressure NVE simulations denoted GF_n_Ar. It is evident from these figures that, in most of the cases, e.g., GF_1_x, GF_2_x, GF_5_x, GF_6_x, GF_8_x, and GF_9_x, all or most of the antenna carbon atoms fall off very fast, namely within ∼20 ps of simulations, consistent with our previous simulations.[19,23] The time of final antenna falloff, defined as the time when #C$_{cluster}$ becomes identical for the first time with #C$_{cage}$, the change in the number of cage carbon atoms during the simulation Δ#C$_{cage}$ = #C$_{cage}$(1210 ps) − #C$_{cage}$(0 ps) and the overall C$_2$ ejection, capture, and cage growth rates are given in Table 4. The cage growth rate is simply the sum of C$_2$ ejection and capture rates. In some cases, complete antenna falloff occurs after a relatively long time, e.g., 50 and 54 ps in GF_3_VS and GF_9_Ar, respectively. However, no original antenna remained attached to any cage over the full simulation time, and all antennas present at the time end points of the trajectories were created by carbon fragment capture.

The average carbon atom temperature profiles for GF_6 and GF_8 simulations during the course of simulations are shown in Figure 2a,b, respectively. It is apparent from these figures that the temperature fluctuation in the case of NVT simulations is much smaller (∼50 K) compared to simulations including buffer gas atoms (∼250 K or more). It is observed that the antenna falloff event occurs faster when simulations are performed including buffer gas in the model system as compared to simulations using NVT. Overall, NVE simulations including buffer gas show higher numbers of C$_2$ pop-out and carbon fragment incorporation events compared to NVT simulations. The greater temperature fluctuation in NVE simulations may be responsible for this difference. The velocity scaling in the NVT simulation is forcing the system to maintain the average kinetic energy of the system more strictly without creating a locally hot region in the system than the explicit collisions with noble gas molecules. Another possible reason might be the different pressure. Assuming the ideal gas, which may not be exact, estimated pressures lie between 219 and 106 atm for C$_{184}$ and C$_{89}$, respectively, and those

Table 4. Cage Sizes at Beginning and End Points of Trajectories, the Change $\Delta\#C_{cage}$, Time of Final Antenna Falloff Event,[a] Ejection Rates, Capture Rates, and Overall Growth Rates

	#C_{cage}			time of antenna	ejection rate	capture rate	growth rate
trajectory name	0 ps	1210 ps	$\Delta\#$ C_{cage}	falloff (ps)	(atoms/ns)	(atoms/ns)	(atoms/ns)
GF_1_VS	120	125	+5	20	0.826	4.959	+4.132
GF_1_He	120	128	+8	9	4.959	11.570	+6.612
GF_1_Ar	120	124	+2	20	5.785	9.091	+3.306
GF_2_VS	149	148	−1	2	0.826	0.000	−0.826
GF_2_He	149	148	−1	6	0.826	0.000	−0.826
GF_2_Ar	149	148	−1	6	0.826	0.000	−0.826
GF_3_VS	135	140	+5	50	0.826	8.263	+7.438
GF_3_He	135	132	−3	30	5.785	6.612	+0.826
GF_3_Ar	135	132	−3	31	4.132	4.959	+0.826
GF_4_VS	160	162	+2	36	4.132	5.785	+1.653
GF_4_He	160	156	−4	8	6.612	3.306	−3.306
GF_4_Ar	160	162	+2	5	4.959	6.612	+1.653
GF_5_VS	76	75	−1	3	3.306	2.479	−0.826
GF_5_He	76	77	+1	6	4.959	5.785	+0.826
GF_5_Ar	76	77	+1	5	4.132	4.959	+0.826
GF_6_VS	131	130	+1	3	0.826	0.000	−0.826
GF_6_He	131	122	−9	3	7.438	0.000	−7.438
GF_6_Ar	131	125	−6	2	4.959	0.000	−4.959
GF_7_VS	130	130	+0	4	1.653	1.653	+0.000
GF_7_He	130	118	−12	5	9.917	0.000	−9.917
GF_7_Ar	130	122	−8	4	6.612	0.000	−6.612
GF_8_VS	102	124	+12	18	0.000	18.182	+18.182
GF_8_He	102	118	+10	17	3.306	16.529	+13.223
GF_8_Ar	102	124	+16	11	1.653	19.835	+18.182
GF_9_VS	80	125	+45	20	5.785	42.975	+37.190
GF_9_He	80	119	+39	6	23.141	54.546	+31.405
GF_9_Ar	80	128	+48	54	13.223	52.893	+39.669
GF_10_VS	88	90	+2	3	0.826	2.479	+1.653
GF_10_He	88	88	+0	4	10.744	10.744	+0.000
GF_10_Ar	88	98	+10	3	2.479	10.744	+8.265

[a] Time when #$C_{cluster}$ = #C_{cage} for the first time.

including buffer gas are 815 and 702 atm, respectively. Collision frequencies at experimental pressures are certainly much lower. At the end of the simulations, mainly C_2 species are present in the system besides the fullerene cage, although occasionally some larger species like C_4–C_9 were also found. Besides C_2, C_4 is the most commonly occurring species. All carbon fragments are linear polyyne chains, and no macrocyclic rings were formed, consistent with high temperature magnifying the effect of entropy.

Table 3 shows also the effect of annealing on cage ring composition. The comparison between the number of rings present in initial and final cages shows that upon high-temperature annealing hexagons are significantly increased and the number of heptagons and octagons are correspondingly decreased. The effect of defect healing is more prominent in the case of the NVE simulations, as the ratio of #six-membered rings to the sum of #five-membered rings, #seven-membered rings, and #eight-membered rings increases faster when compared with simulations using a velocity scaling thermostat.
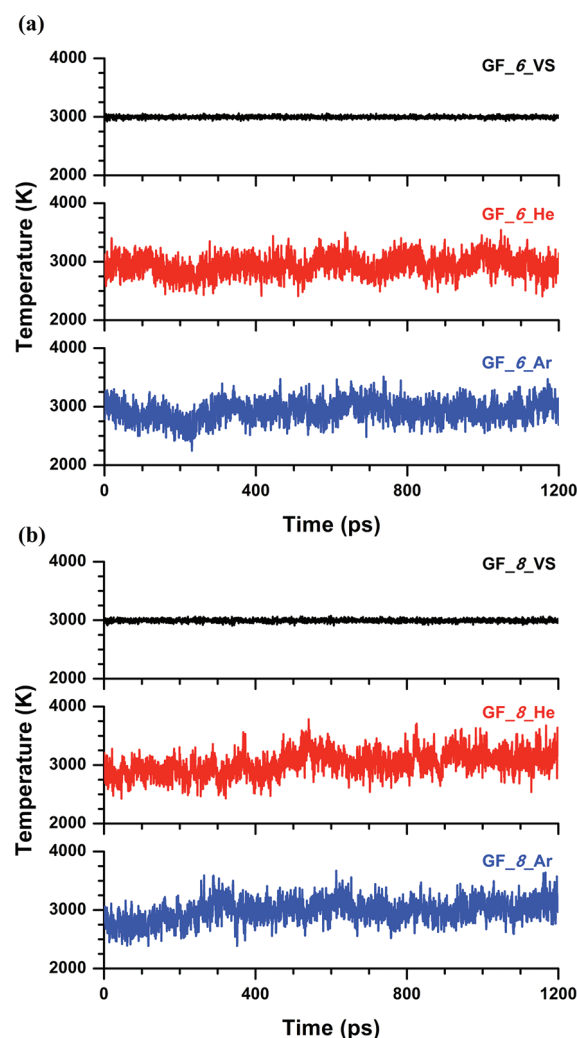
(a)

(b)

Figure 2. Average C temperature evolution with different thermostat conditions.

3.B. Shrinking Mechanism. The shrinking mechanism was described in detail in our previous work.[23] Thus, we describe the shrinking mechanism in the present simulations only briefly by giving examples from the GF_6_He trajectory in Figure 3. At first we discuss antenna falloff, and Figure 3a,b shows two such events. The initial GF_6 giant fullerene possesses two short C_2 antennas. In the snapshot taken at 0.00 ps simulation time, one can clearly see one C_2 unit being attached to an sp³-hybridized cage C atom, which was simultaneously part of two hexagons and a heptagon (Figure 3a). At 0.20 ps, this C_2 detached from the cluster. Figure 3b shows a similar situation with the second C_2 being attached to an sp³-hybridized cage C atom that was simultaneously part of a pentagon and two hexagons. Here, it took 1.82 ps for the antenna to disconnect from the GF cage. The second stage of the shrinking process, namely C_2 pop-out, often resembles the "window mechanism" described by Xu et al. in 1994 on the basis of TBMD simulations of C_2 elimination from C_{60} at ∼6000 K.[53] We have described such C_2 pop-out in detail in ref 23; however, the window mechanism is not the only C_2 elimination mechanism occurring in DFTB-based MD simulations. Figure 3c shows a sequence of events leading up to C_2 elimination from a divalent carbon (in the following named "carbene") defect. There are four rings participating in
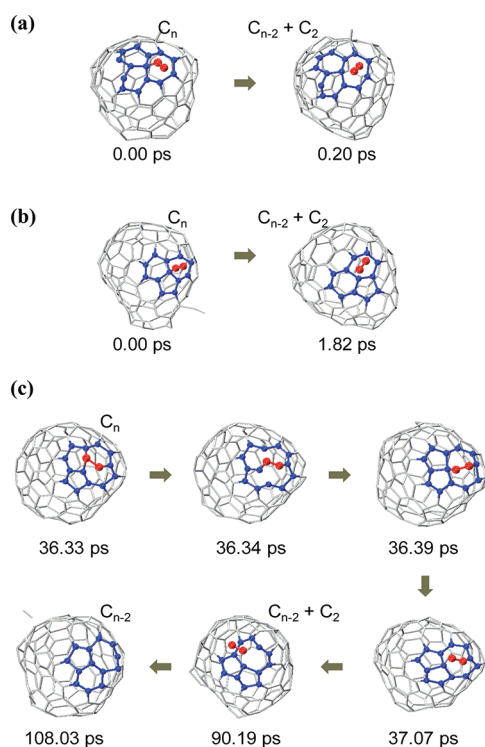
22712

dx.doi.org/10.1021/jp203614e |*J. Phys. Chem. C* 2011, 115, 22707–22716

Figure 3. (a, b) Antenna falloff events. (c) C_2-fragment emission and shrinking mechanism in GF_*6*_He. C atoms are marked blue in the region from where the described event occurs. Antenna C atoms are marked in red. Other C atoms are drawn in gray for clarity.

this ejection, marked in blue: a heptagon, two hexagons, and a pentagon. At first, the seven-membered ring containing the carbene produced a kink at 36.33 ps. The kink site and the four participating rings converted to two joint 10-membered ring-openings, with the carbene defect being converted to a C_3 bridge at 36.34 ps. At 36.39 ps these 10-membered rings converted to two abutting pentagons and two fused 7-membered rings in which the bridge was shortened to two carbons. Around 37.07 ps the bridge broke, and a wobbling C_2 unit was formed. Much later, at around 90.19 ps, this wobbling C_2 broke off, leaving behind a carbene-bearing octagon joint to the two abutting pentagons. Further ring transformations occurred at 108.03 ps when this structure transformed into a carbene-containing 7/5/6 structure. Overall, this process corresponds to a carbene-containing 7/6/6/5 structure transforming into a carbene-containing 7/5/6 structure where one C_2 unit was ejected. The periodic boundary conditions allow future reactions with the fullerene cage and the ejected C_2 molecules, resulting in C_2 capture as described in the next paragraph.

3.C. Growth Mechanism. As discussed already above, cage growth only occurs in trajectories where a sufficient number of carbon fragments were present in the system due to antenna "fall-off", allowing reactions of C_n fragments with the giant fullerene during the simulation time. Representative snapshots of C_2 capture processes are shown in Figures 4 and 5 for GF_*1*_He and GF_*8*_He trajectories, respectively. No significant difference is observed in simulations using different thermal control conditions (VS, He, or Ar). In these figures, the newly added C atoms are indicated in red while the C atoms of the participating ring structures are indicated in blue. We note that C_2 incorporation can occur either via breaking of the original C_2 bond (dissociative, in panels a of Figures 4 and 5, similar to the
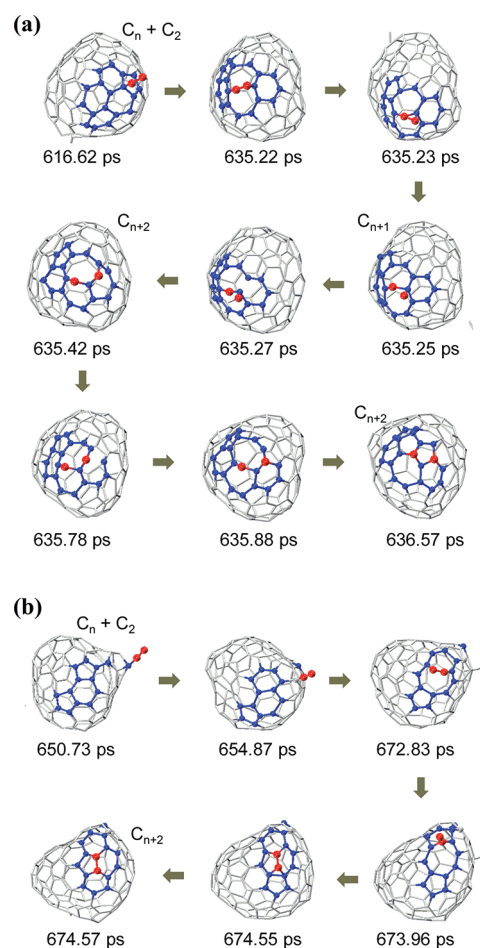

Figure 4. Two different C_2-fragment incorporation events occurring in trajectory GF_*1*_He. Carbon atoms are marked in blue in the region where the described event occurs. Incorporated C atoms are marked in red. Other C atoms are drawn in gray for clarity.

proposed mechanism by Saito et al.[43] shown in Scheme 1 d), or the captured C_2 molecule becomes subsequently "swallowed whole", leaving its original C—C bond intact (nondissociative, in panels b of Figures 4 and 5, similar to the mechanism reported by Murry et al.[51–53] shown in Scheme 1 c). The elementary chemical reactions encountered in our QM/MD simulations are depicted in a more abstract way in Scheme 2, where (a) nondissociative and (b) dissociative pathways start to differ when the attached C_2 unit either dissociates or forms a C_2-bridge. It is observed that in general the C_2 unit is incorporated via three distinct stages: (i) reaction of C_2 with a cage C which is shared by adjacent five- and six-membered rings/five- and seven-membered rings/six- and seven-membered rings (chemisorptions), (ii) large ring formation in which C_2 is attached to form a bridge, and (iii) C_2 consumption by the cage via ring transformation and thus formation of five- and six-membered rings. In some cases the two C's of the C_2 unit are consumed in two steps.

The growth mechanism proceeds in our simulations exclusively by the more probable edge-on attack of C_2 and subsequent cage incorporation as suggested by Murry et al.,[51,52] not by the highly improbable concerted Endo—Kroto insertion mechanisms shown in Scheme 1 a,b. Yi et al.[38] had observed Endo—Kroto insertion in very short CPMD simulations with specifically prepared initial geometries. It turns out that such geometries
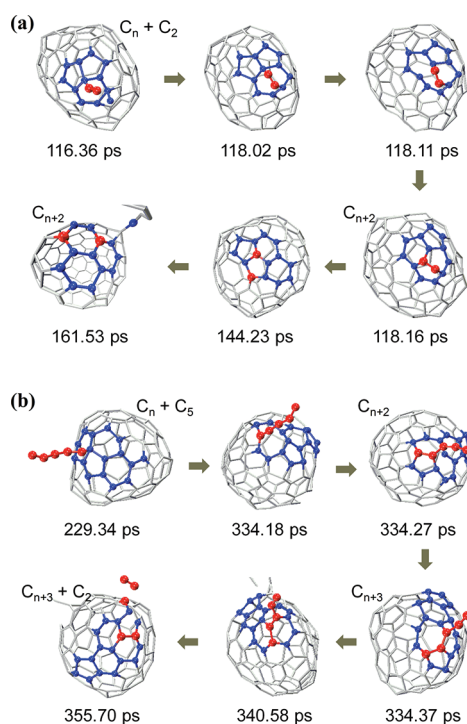
Figure 5. (a) C_2- and (b) C_3-fragment incorporation events occurring in trajectory GF_8_He. Carbon atoms are marked in blue in the region where the described event occurs. Incorporated C atoms are marked in red. Other C atoms are drawn in gray for clarity.

Scheme 2. C_2 Insertion Mechanism Observed in Present QM/MD Simulations of Hot GFs: (a) Nondissociative and (b) Dissociative Insertion Pathway

(a)   (b)
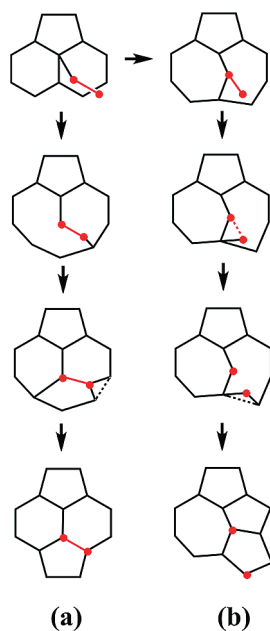
are virtually never realized in actual simulations of hot GF with ensembles of carbon fragments. The reorganization of the exothermic reaction energy due to GF-C_2 bond formation in the carbon network is crucial to achieve a lifetime long enough to proceed via the cage ingestion processes described above. Our simulations show that the cage ingestion occurs on the order of several tens of picoseconds after initial C_2 capture.

4. CONCLUSIONS

Constant temperature/constant density direct quantum chemical/molecular mechanics (QM/MM) molecular dynamics (MD) simulations of dynamically self-assembled, hot giant fullerenes (GFs) with their attached polyyne antennas were performed on the nanosecond time scale to investigate the C_2 ejection and cage incorporation rates associated with GF cage shrinking and growth. In the microcanonical ensemble (NVE simulations) we included explicit ambient buffer gas helium or argon atoms at high pressures, and in constant temperature simulations we employed a velocity scaling thermostat, keeping the system pressure relatively lower. It was found that hot GFs are able to shrink as well as grow during continued high temperature simulations, on the order of several carbon atoms per nanosecond. C_2 ejection followed the previously described routes, namely a stepwise mechanism involving an intermediate sp^3-carbon defect in the vicinity of a polygon larger than a hexagon.[19,23,51−53] C_2 insertion occurred roughly along reverse reaction pathways, where either the whole C_2 unit was ingested forming a temporary bridge structure in a large hole defect (nondissociative pathway, Scheme 2 a), or the C_2 unit suffered dissociation of the C−C bond and individual adsorption of the two carbon atoms (dissociative pathway, Scheme 2 b). These reactions resemble, but are not identical to, previously proposed and described stepwise nondissociative[51,52] (Scheme 1 c) and dissociative[43] (Scheme 1 d) insertion/emission mechanisms involving intermediate sp^3 defects; however, a concerted insertion or removal of C_2 into six-membered rings as in the proposed Endo−Kroto mechanism[41,44] (Scheme 1 a,b) was not observed in our simulations.

It was observed that larger GFs (>100 cage carbons) have a tendency to shrink whereas smaller GFs (<100 cage carbons) tend to grow (see Table 4). However, the C_2 ejection and insertion rates depend strongly on the concentration of available carbon outside the cages: A larger number of free carbons increases the growth rate, whereas a smaller number increases the shrinking rate. Our observation supports the notion that for a constant carbon density there exists a dynamic equilibrium with a temporally stable, symmetric GF cage size distribution, as discussed by Curl et al.[13] However, we find that the presence of explicit buffer gas and the resulting higher pressure favor the shrinking process, in agreement with experimental increased yield for C_{60} and C_{70} with higher buffer gas pressure.[1]

In our original "shrinking hot giant" (SHG) road of fullerene formation, we neglected the possibility of cage growth as our "size-down" simulations were always performed in vacuum, where the concentration of noncage carbon fragments was effectively zero. This is certainly an extreme oversimplification. In laser or arc discharge fullerene synthesis, the carbon vapor plume expands and is cooled by the buffer gas, so that the carbon concentration only gradually decreases. Our simulations suggest that, under this negative carbon density gradient, GFs will tend to shrink. The energy required for the endothermic shrinking process is available, since the formation of GFs is highly exothermic and the experiments are typically performed in a furnace. Our simulations suggest, as we and others have noted before,[20,60,61] that C_{60}/C_{70} formation under typical conditions is a kinetically

22714

dx.doi.org/10.1021/jp203614e |J. Phys. Chem. C 2011, 115, 22707–22716

controlled process. On the other hand, the present simulations can explain the fact that fullerene molecules can grow inside carbon nanotubes,[36] and that fullerene coalescence[37] experiments in a *tightly sealed environment* can produce oligomers with a higher number of carbon atoms as present in the component monomers.

Perhaps most intriguingly, we may conjecture that C_2 swapping between GFs after cage self-assembly may lead to total replacement of all constituent carbon atoms of the initial GF cage, since the experimental time of fullerene synthesis is on the order of 1000 microseconds.[62] If this should indeed happen, it becomes literally true that fullerene cages are dissipative structures formed under nonequilibrium conditions, similar to atmospheric clouds or biological systems. This would then be the first time that the formation of a molecular, covalently bound structure is explained in terms of Prigogine's theory of self-organization in nonequilibrium systems.[9,10]

■ ASSOCIATED CONTENT

ⓢ **Supporting Information.** Cluster and cage size evolution of trajectories GF_n (n = 2, 3, 4, 5, 9, and 10) as a function of time with different temperature and pressure conditions. Average atomic carbon temperature as a function of time with different thermostat and pressure conditions for trajectories GF_n (n = 1 and 7). Depictions and Cartesian coordinates of initial and final carbon clusters of all 30 trajectories. QuickTime movies of C_2 ejection and incorporation processes shown in Figures 4 and 5a,b. This material is free of charge via the Internet at http://pubs.acs.org.

■ AUTHOR INFORMATION

Corresponding Author
*E-mail: sirle@iar.nagoya-u.ac.jp (S.I.), morokuma@fukui.kyoto-u.ac.jp (K.M.).

Present Addresses
§Department of Chemistry, Northwestern University, Evanston, IL 60208.

■ ACKNOWLEDGMENT

■ REFERENCES

(1) Kroto, H. W.; Heath, J. R.; O'Brien, S. C.; Curl, R. E.; Smalley, R. E. *Nature* **1985**, *318*, 162.

(2) Johnson, M. P.; Donnet, J. B.; Wang, T. K.; Wang, C. C.; Locke, R. W.; Brinson, B. E.; Marriott, T. *Carbon* **2002**, *40*, 189.

(3) Zhang, Q. L.; O'Brien, S. L.; Heath, J. R.; Liu, Y.; Kroto, H. W.; Smalley, R. E. *J. Phys. Chem.* **1986**, *90*, 525.

(4) Kroto, H. W.; McKay, K. *Nature* **1988**, *331*, 328.

(5) Heath, J. R. In *ACS Symposium Series No. 481*; American Chemical Society: Washington, DC, 1991.

(6) Wakabayashi, T.; Achiba, Y. *Chem. Phys. Lett.* **1992**, *190*, 465.

(7) Smalley, R. E. *Acc. Chem. Res.* **1992**, *25*, 98.

(8) vonHelden, G.; Gotts, N. G.; Bowers, M. T. *Nature* **1993**, *363*, 60.

(9) Nicolis, G.; Prigogine, I. *Self-Organization in Nonequilibrium Systems: From Dissipative Structures to Order Through Fluctuations*; Wiley: New York, 1977.

(10) Prigogine, I.; Stengers, I. *Order out of Chaos: Man's New Dialogue with Nature*; Bantam Books: Toronto, 1984.

(11) Whitesides, G. M.; Grzybowski, B. *Science* **2002**, *295*, 2418.

(12) Fialkowsy, M.; Bishop, K. J. M.; Klajn, R.; Smoukov, S. K.; Campbell, C. J.; Grzybowski, B. A. *J. Phys. Chem. B* **2006**, *110*, 2482.

(13) Curl, R. F.; Lee, M. K.; Scuseria, G. E. *J. Phys. Chem. A* **2008**, *112*, 11951.

(14) Porezag, D.; Frauenheim, T.; Köhler, C.; Seifert, G.; Kaschner, R. *Phys. Rev. B* **1995**, *51*, 12947.

(15) Elstner, M.; Porezag, D.; Jungnickel, G.; Elsner, J.; Haugk, M.; Frauenheim, T.; Suhai, S.; Seifert, G. *Phys. Rev. B* **1998**, *58*, 7260.

(16) Irle, S.; Zheng, G.; Elstner, M.; Morokuma, K. *Nano Lett.* **2003**, *3*, 465.

(17) Irle, S.; Zheng, G.; Elstner, M.; Morokuma, K. *Nano Lett.* **2003**, *3*, 1657.

(18) Zheng, G.; Irle, S.; Elstner, M.; Morokuma, K. *J. Phys. Chem. A* **2004**, *108*, 3182.

(19) Zheng, G.; Irle, S.; Morokuma, K. *J. Chem. Phys.* **2005**, *122*, 014708/1.

(20) Irle, S.; Zheng, G.; Wang, Z.; Morokuma, K. *J. Phys. Chem. B* **2006**, *110*, 14531.

(21) Irle, S.; Zheng, G.; Wang, Z.; Morokuma, K. *Nano* **2007**, *2*, 21.

(22) Saha, B.; Shindo, S.; Irle, S.; Morokuma, K. *ACS Nano* **2009**, *3*, 2241.

(23) Zheng, G.; Wang, Z.; Irle, S.; Morokuma, K. *J. Nanosci. Nanotechnol.* **2007**, *7*, 1662.

(24) Curl, R. F.; Smalley, R. E. *Sci. Am.* **1991**, *265*, 54.

(25) Bogana, M.; Ravagnan, L.; Casari, C. S.; Zivelonghi, A.; Baserga, A.; Bassi, A. L.; Bottani, C. E.; Vinati, S.; Salis, E.; Piseri, P.; Barborini, E.; Colombo, L.; Milani, P. *New J. Phys.* **2005**, *7*, 1.

(26) Yamaguchi, Y.; Colombo, L.; Piseri, P.; Ravagnan, L.; Milani, P. *Phys. Rev. B* **2007**, *76*, 134119/1.

(27) Ueno, Y.; Saito, S. *Phys. Rev. B* **2008**, *77*, 085403/1.

(28) Bates, K. R.; Scuseria, G. E. *Theor. Chem. Acc.* **1998**, *99*, 29.

(29) Dolgonos, G. A.; Peslherbe, G. H. *Chem. Phys. Lett.* **2004**, *398*, 217.

(30) Dolgonos, G. A.; Peslherbe, G. H. *Int. J. Mass Spectrom.* **2005**, *241*, 261.

(31) Dunlap, B. I. *Int. J. Quantum Chem.* **1997**, *64*, 193.

(32) Calaminici, P.; Geudtner, G.; Koser, A. M. *J. Chem. Theory Comput.* **2009**, *5*, 29.

(33) Guangshi, T.; Hengjian, Z.; Chuanbao, C.; Rongzhi, L.; Hesun, Z. *J. Beijing Inst. Technol.* **1995**, *4*, 141.

(34) Huang, J. Y.; Ding, F.; Jiao, K.; Yakobson, B. I. *Phys. Rev. Lett.* **2007**, *99*, 175503/1.

(35) Chuvilin, A.; Kaiser, U.; Bichoutskaia, E.; Besley, N. A.; Khlobystov, A. N. *Nat. Chem.* **2010**, *2*, 450.

(36) Koshino, M.; Niimi, Y.; Nakamura, E.; Kataura, H.; Okazaki, T.; Suenaga, K.; Iijima, S. *Nat. Chem.* **2010**, *2*, 117.

(37) Hansen, K.; Yeretzian, C.; Whetten, R. L. *Chem. Phys. Lett.* **1994**, *218*, 462.

(38) Yi, J.-Y.; Bernholc, J. *Phys. Rev. B* **1993**, *48*, 5724.

(39) Huang, R.; Li, H.; Lu, W.; Yang, S. *Chem. Phys. Lett.* **1994**, *228*, 111.

(40) Hammond, M. R.; Zare, R. N. *Geochim. Cosmochim. Acta* **2008**, *72*, 5521.

(41) Endo, M.; Kroto, H. W. *J. Phys. Chem.* **1992**, *96*, 6941.

(42) O'Brien, S. C.; Heath, J. R.; Curl, R. F.; Smalley, R. E. *J. Chem. Phys.* **1988**, *88*, 220.

(43) Saito, R.; Dresselhaus, G.; Dresselhaus, M. S. *Chem. Phys. Lett.* **1992**, *195*, 537.

(44) Yoshida, M.; Osawa, E. *Bull. Chem. Soc. Jpn.* **1995**, *68*, 2083.

(45) Kroto, H. W. *Nature* **1987**, *384*, 529.

(46) Brinkmann, G.; Franceus, D.; Fowler, P. W.; Graver, J. E. *Chem. Phys. Lett.* **2006**, *428*, 386.

(47) Khan, S. D.; Ahmad, S. *Nanotechnology* **2006**, *17*, 4654.

(48) Jin, C.; Lan, H.; Suenaga, K.; Peng, L.; Iijima, S. *Phys. Rev. Lett.* **2008**, *101*, 176102/1.

(49) Budyka, M. F.; Zyubina, T. S.; Ryabenko, A. G. *Int. J. Quantum Chem.* **2001**, *88*, 652.

(50) Budyka, M. F.; Zyubina, T. S.; Ryabenko, A. G.; Muradyan, V. E.; Esipov, S. E.; Cherepanova, N. I. *Chem. Phys. Lett.* **2002**, *354*, 93.

(51) Murry, R. L.; Strout, D. L.; Odom, G. K.; Scuseria, G. E. *Nature* **1993**, *366*, 665.

(52) Murry, R. L.; Strout, D. L.; Scuseria, G. E. *Int. J. Mass Spectrom. Ion Processes* **1994**, *138*, 113.

(53) Xu, C. X.; Scuseria, G. E. *Phys. Rev. Lett.* **1994**, *72*, 669.

(54) Osawa, E.; Yoshida, M.; Ueno, H.; Sage, S.; Yoshida, E. *Fullerene Sci. Technol.* **1999**, *7*, 239.

(55) Saha, B.; Irle, S.; Morokuma, K. *J. Chem. Phys.* **2010**, *132*, 224303/1.

(56) Seifert, G.; Porezag, D.; Frauenheim, T. *Int. J. Quantum Chem.* **1996**, *58*, 185.

(57) Carlos, W. E.; Cole, M. W. *Surf. Sci.* **1980**, *91*, 339.

(58) Zahn, D.; Seifert, G. *J. Phys. Chem. B* **2004**, *108*, 16495.

(59) Carlborg, C. F.; Shiomi, J.; Maruyama, S. *Phys. Rev. B* **2008**, *78*, 205406.

(60) Curl, R. F. *Philos. Trans. R. Soc. London Ser. A* **1993**, *343*, 19.

(61) Fedorov, A. S.; Fedorov, D. A.; Kuzubov, A. A.; Avramov, P. V.; Nishimura, Y.; Irle, S.; Witek, H. A. *Phys. Rev. Lett.* **2011**, *107*, 175506/1.

(62) Suzuki, S.; Yamaguchi, H.; Ishigaki, T.; Kataura, H.; Kratschmer, W.; Achiba, Y. *Eur. Phys. J. D* **2001**, *16*.